New Biodegradable Blends Prepared from Polylactide, Titanium Tetraisopropylate, and Starch

Hsin-Tzu Liao, Chin-San Wu

Department of Chemical and Biochemical Engineering, Kao Yuan University, Kaohsiung County, Taiwan 82151, Republic of China

Received 8 June 2007; accepted 17 December 2007
DOI 10.1002/app.27901
Published online 8 February 2008 in Wiley InterScience (www.interscience.wiley.com).

ABSTRACT: In this study, new biodegradable nanocomposites were prepared from poly(lactic acid) (PLA) or acrylic acid grafted poly(lactic acid) (PLA-*g*-AA), titanium tetraisopropylate, and starch by means of an *in situ* sol–gel process and the melt-blending method. The samples were characterized with X-ray diffractometry, Fourier transform infrared spectroscopy, differential scanning calorimetry, thermogravimetric analysis, scanning electron microscopy, and an Instron mechanical tester. According to the results, a PLA-*g*-AA/TiO_2 hybrid could improve the properties of a PLA/TiO_2 hybrid because the carboxylic acid groups of acrylic acid should act as coordination sites for the titania phase to form the Ti—O—C chemical bond. It was also found that both the tensile strength and glass-transition temperature increased to a maximum value and then decreased with increasing TiO_2 because excess particles (e.g., greater than 10 wt % TiO_2) could cause separation or segregation between the organic and inorganic phases. A PLA-*g*-AA/TiO_2/starch hybrid could obviously enhance the mechanical properties of a PLA-*g*-AA/starch hybrid because the former could provide a smaller starch phase size and nanoscale dispersion of TiO_2 in the polymer matrix. The biodegradable nanocomposites produced in our laboratory could provide a plateau tensile strength at break when the starch content was up to 50 wt %. © 2008 Wiley Periodicals, Inc. J Appl Polym Sci 108: 2280–2289, 2008

Key words: biodegradable; blends; FTIR; thermal properties; X-ray

INTRODUCTION

It is now possible to combine polymers and ceramics via molecular-level manipulation with a sol–gel process to create novel materials.[1–12] The promise of these new hybrid materials is a controllable combination of the benefits of polymers (e.g., flexibility, toughness, and easy processing) and ceramics or glass (e.g., hardness, durability, and thermal stability). In synthesizing an organic–inorganic composite, the organic polymer generally is subjected to inorganic modification; that is, the organic polymer is the dominant phase.[13,14] Examples of organic polymers used in the sol–gel process include elastomers, glassy polymers, semicrystalline polymers, and membranes of perfluorosulfonic acid.[15] Ceramic precursors are usually organometallic compounds [$M(OC_nH_{2n+1})_z$, where M is Si, Sn, Ti, Zr, Al, etc.].[14,16,17]

It is well known that some factors, such as the particle size of the inorganic phase, the uniform distribution of the inorganic phase within the organic phase, and the interfacial forces between the two phases, can significantly affect the microstructures and properties of hybrid materials. The formation of hydrogen or covalent bonds between the two phases is normally used to establish this interfacial force.[15,16] In general, a hydrogen bond can arise from the basic group of the hydrogen acceptor in the polymer and the hydroxyl group of the intermediate species of metal alkoxides, whereas a covalent bond can be formed through the reaction of hydroxyl or carboxyl groups in the polymer with residual metal-bonded organic groups in the inorganic network.

In response to the increasing public awareness of the environmental hazards caused by the disposal of plastics, a great deal of research has been focused on the development and use of alternative biodegradable plastic materials. Poly(lactic acid) (PLA), a linear aliphatic thermoplastic polyester, is one of the most popular biodegradable polymers. At present, the applicability of PLA is somewhat limited because of the quite high price and low deformation at break. Considerable efforts have been made to improve this polymer to compete with low-cost and flexible commodity polymers. These efforts involve either modifying PLA with biocompatible plasticizers or blending PLA with other cheap and biodegradable natural biopolymers (e.g., starch, wood flour, cellulose, and chitin). Various types of chemicals or plasticizers [e.g., citrate esters, poly(ethylene glycol), glucose monoesters, and partial fatty acid

Correspondence to: H.-T. Liao (htliaw@cc.kyu.edu.tw).
Contract grant sponsor: National Science Council of the Republic of China; contract grant number: NSC-94-2622-E-244-004-CC3.

esters] have been tried to improve the flexibility and impact resistance of PLA.[18–21] The resulting plasticized PLA materials are improved in terms of deformation and resilience. In blending with other polymers, the other polymers include aliphatic polyesters such as poly(ε-caprolactone),[22] poly(glycolic acid),[23] and poly(hydroxy butyrate).[24,25] Despite an effective improvement of the biodegradability, these blends have been found to be immiscible, and this results in fairly poor mechanical properties.

The purpose of this article is the preparation of biodegradable PLA/TiO_2/starch nanocomposites by an *in situ* sol–gel process and the simple melt-blending method to mitigate the disadvantages of PLA. The conclusions are based on a combination of Fourier transform infrared (FTIR) spectrophotometry, scanning electron microscopy (SEM), X-ray diffractometry (XRD), differential scanning calorimetry (DSC), thermogravimetric analysis (TGA), and an Instron mechanical tester.

EXPERIMENTAL

Materials

Polylactide, composed of 95% L-lactide and 5% *meso*-lactide, was used as supplied by Cargill-Dow Corp. (Minnetonka, MN) Acrylic acid (AA), a commercial product of Aldrich Chemical Corp. (Milwaukee, WI), was purified by recrystallization from chloroform before use. The initiator benzoyl peroxide (BPO; Aldrich Chemical) was purified by dissolution in chloroform and reprecipitation with methanol. The starch, composed of 27% amylose and 73% amylopectin, was obtained from Sigma Chemical Corp. (Steinheim, Germany). Titanium tetraisopropylate (TTIP; $Ti[OCH(CH_3)_2]_4$; >97%; Merck Chemical Co., Whitehouse Station, NJ) was used as received. Other reagents were purified by the conventional methods. The acrylic acid grafted poly(lactic acid) (PLA-*g*-AA) copolymer was synthesized in our laboratory as described next.

Sample preparation

PLA-*g*-AA copolymer

The grafting reaction of AA onto PLA was performed with xylene as an interfacial agent and BPO as an initiator under a nitrogen atmosphere at 85 ± 2°C. The reaction lasted for 6 h with a rotor speed of 60 rpm. The grafting percentage was determined by a titration method,[26] and the result showed that it was about 5.96 wt % when the BPO and AA loadings were kept at 0.3 and 10 wt %, respectively. More information about the grafting reaction of AA onto PLA can be found in our previous works.[27,28]

TABLE I
Compositions of Various Sol–Gel Liquid Solutions for the Preparation of the Hybrid Materials

	TiO_2 (wt %)				
	3	7	10	12	15
Polymer[a]	38.80	37.20	36.00	35.20	34.00
TTIP (g)	4.26	9.93	14.18	16.90	21.26
Isopropyl alcohol/[TTIP][b]	17	17	17	17	17
Sol A					
[Acetic acid]/[TTIP][b]	0.01	0.01	0.01	0.01	0.01
[HCl]/[TTIP][b]	0.08	0.08	0.08	0.08	0.08
[H_2O]/[TTIP][b]	4.0	4.0	4.0	4.0	4.0

[a] The polymers were PLA, PLA-*g*-AA, PLA–starch, and PLA-*g*-AA–starch.
[b] The molar ratio of isopropyl alcohol, acetic acid, HCl, or H_2O to TTIP.

Preparation of hybrids from PLA, PLA-*g*-AA, TiO_2, and starch

A mixture, called Sol A, was prepared by the dissolution of a stoichiometric amount of TTIP, H_2O, HCl (as the catalyst), and acetic acid in isopropyl alcohol (Table I) with stirring at room temperature for 30 min to obtain a homogeneous solution. According to Table I, a predetermined amount of PLA, PLA-*g*-AA, PLA–starch, or PLA-*g*-AA–starch was put into a Brabender Plastograph 200 Nm Mixer W50EHT instrument (Duisburg, Germany) with a blade-type rotor to melt it with the rotor speed and blending temperature kept at 50 rpm and 190–200°C, respectively. When the polymer had melted completely, Sol A was added to continue the sol–gel process for another 20 min. Before characterization, each sample was dried at 105°C in a vacuum oven for 3 days to remove residual solvents. The hybrid products were pressed into a thin plate by a hot press at 190°C and then were put into a dryer for cooling. Next, the cool thin plate was made into standard specimens for characterization.

Characterization of the hybrids

FTIR analysis

An FTIR spectrophotometer (FTS-7PC type, Bio-Rad, Madison, WI), using thin-film samples, was used to investigate the graft reaction of AA onto PLA and to verify the incorporation of a titania phase to the extent that Ti—O—Ti and Ti—O—C bonds were formed in hybrids.

XRD analysis

XRD intensity curves were recorded with a Rigaku (Tokyo, Japan) D/max 3V X-ray diffractometer with Cu Kα radiation at a scanning rate of 2°/min to

study the structural changes between PLA, PLA-*g*-AA, and hybrids.

DSC analysis

The melting temperature (T_m) and glass-transition temperature (T_g) of the samples were determined with a TA Instrument (New Castle, DE) 2010 DSC system. For DSC tests, sample sizes ranged from 4 to 6 mg, and the T_m and T_g values were obtained from the melting curves taken at a temperature range of −30 to 250°C scanned at a heating rate of 10°C/min.

TGA

A thermogravimetric analyzer (2010 TGA, TA Instrument) was used to assess whether organic–inorganic phase interactions influenced the thermal degradation of the hybrids. Samples were placed in alumina crucibles and tested with a thermal ramp over the temperature range of 30–600°C at a heating rate of 20°C/min. The initial decomposition temperature ($T_{d,\text{initial}}$) and maximum decomposition temperature ($T_{d,\text{max}}$) of the hybrids were obtained from the mass loss (thermogravimetry percentage) and derivative mass loss (derivative thermogravimetry) curves.

Hybrid morphology

A scanning electron microscope (model S-1400, Hitachi, Noka, Japan) was used to study the morphology of the hybrids and to measure the starch phase size in the polymers. Before testing, hybrids were prepared as thin films with a hydrolytic press, and the films were treated with hot water at 80°C for 24 h. Afterward, the films were coated with gold and observed with SEM.

Mechanical testing

An Instron mechanical tester (Lloyd model, LR5K type, Segensworth, Fareham, UK), following the ASTM D 638 method, was used to measure the tensile strength and elongation at break of the blends. The test films were conditioned at 50 ± 5% relative humidity for 24 h and then tested at a 20 mm/min crosshead speed. Each blend was tested with five samples, and the results were averaged to obtain a mean value.

RESULTS AND DISCUSSION

XRD

In this study, XRD analysis was used to study the crystalline structures of pure PLA, PLA-*g*-AA, and PLA-*g*-AA/TiO_2. The XRD pattern of pure PLA [Fig. 1(A)] shows that there are two peaks at about 2θ = 16.9° and 2θ = 19.5°. This result is similar to that reported by Tsuji et al.[29] and in our previous study.[27] For the PLA/TiO_2 hybrid versus the pure PLA, it is clear that there are three new peaks at about 2θ = 22.6°, 2θ = 26.2°, and 2θ = 29.2° in its XRD pattern [Fig. 1(B)]. The appearance of a peak at 22.6° may be due to the Ti_2O_3 phase of the titania network, and the new peaks at about 26.2 and 29.2° may be due to the anatase or rutile phase of the crystalline structure of TiO_2.[30] A comparison of the XRD patterns of PLA/TiO_2 and PLA-*g*-AA/TiO_2 [Fig. 1(B,C)] reveals a new peak in the latter at about 2θ = 18.2°. This new peak at 2θ = 18.2°, also identified by Shogren et al.,[31] may be due to the formation of an ester carbonyl functional group through the reaction between carboxylic acid groups of PLA-*g*-AA and titanol groups of the titania network and provides evidence that the presence of AA changes the crystalline structure of the PLA/TiO_2 hybrid. The formation of an ester carbonyl functional group is further described in the following discussion of FTIR analysis.

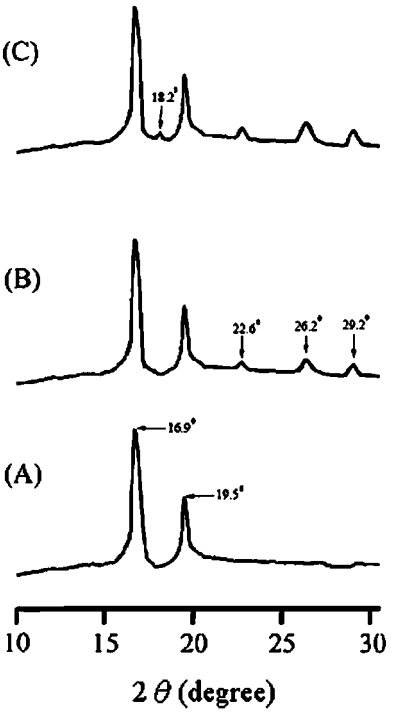

Figure 1 XRD spectra in the limited range of 10–35° for (A) pure PLA, (B) PLA/TiO_2 (10 wt %), and (C) PLA-*g*-AA/TiO_2 (10 wt %).

IR spectroscopy

Figures 2–4 illustrate FTIR spectra of PLA, PLA-*g*-AA, PLA/TiO_2 (10 wt %), and PLA-*g*-AA/TiO_2 (10 wt %) in the 2500–4000-, 1700–1800-, and 500–1700-cm^{-1} ranges, respectively. All the characteristic

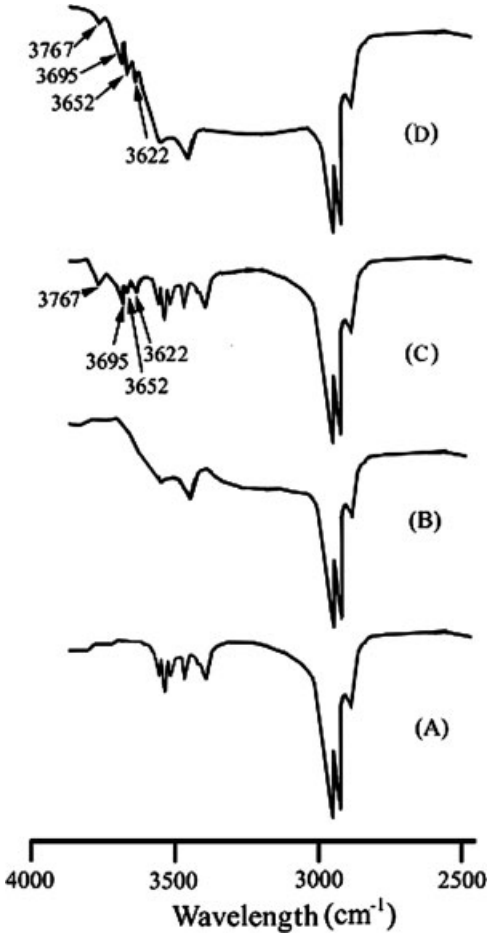

Figure 2 FTIR spectra in the limited range of 2500–4000 cm^{-1} for (A) pure PLA, (B) PLA-*g*-AA, (C) PLA/TiO_2 (10 wt %), and (D) PLA-*g*-AA/TiO_2 (10 wt %).

peaks of PLA at 3300–3800, 2800–2958, 1700–1760, and 500–1500 cm^{-1} appear in the four polymers,[28,32] revealing that the major structure of the polymer is not altered during the preparation of the hybrids, but an extra peak can be observed for the modified PLA at 1710 cm^{-1} [Fig. 3(B)], which is assigned to —C=O, as well as a broad O—H stretching absorbance at 3000–3300 cm^{-1}. Similar results have been reported elsewhere.[27,33] This pattern of peaks demonstrates that AA was grafted onto PLA because the discernible shoulder near 1710 cm^{-1} revealed the formation of free acid in the modified polymer.

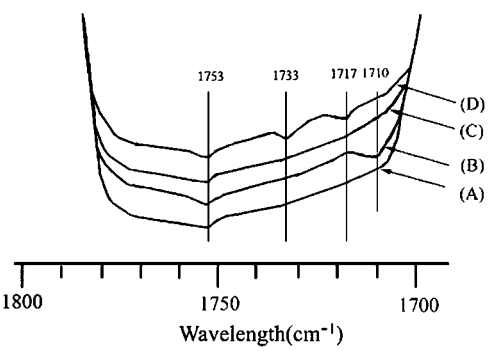

Figure 3 FTIR spectra in the limited range of 1700–1800 cm^{-1} for (A) pure PLA, (B) PLA-*g*-AA, (C) PLA/TiO_2 (10 wt %), and (D) PLA-*g*-AA/TiO_2 (10 wt %).

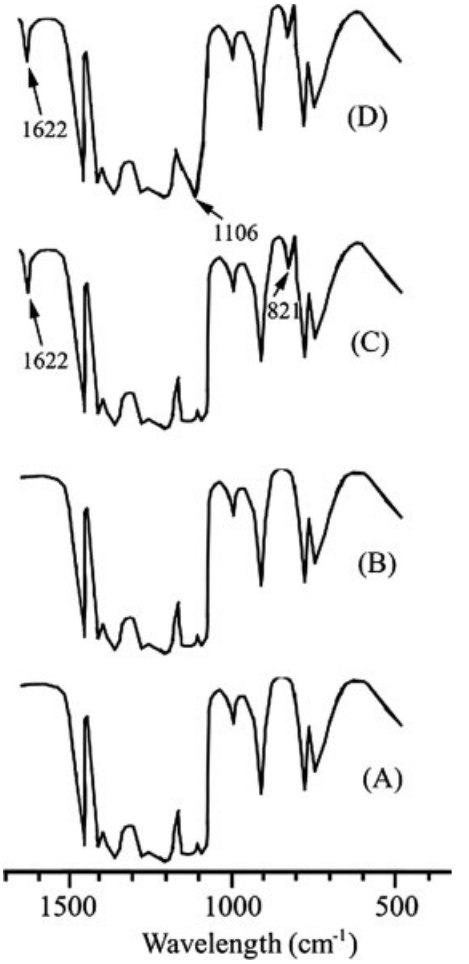

Figure 4 FTIR spectra in the limited range of 500–1700 cm^{-1} for (A) pure PLA, (B) PLA-*g*-AA, (C) PLA/TiO_2 (10 wt %), and (D) PLA-*g*-AA/TiO_2 (10 wt %).

A comparison of the FTIR spectra of PLA and PLA/TiO_2 (10 wt %) shows new peaks at 3622, 3652, 3695, and 3767 cm^{-1} [Fig. 2(C)] and at 821 and 1622 cm^{-1} [Fig. 4(C)] in the latter. The extra bands at 3622, 3652, and 3695 cm^{-1} indicate characteristic tetrahedral coordinated vacancies and are designated as $_4Ti^{4+}$—OH. A further band at 3767 cm^{-1} is assigned to octahedral vacancies and designated as $_6Ti^{3+}$—OH. This region at 3600–3800 cm^{-1} is therefore identified as being representative of non-hydrogen-bonded hydroxyl groups (labeled as isolated or free hydroxyl groups). The peaks at 821 and 1622 cm^{-1} are assigned to the Ti—O and Ti—O—Ti stretching modes.[34,35]

For the PLA-*g*-AA/TiO_2 hybrid versus the PLA/TiO_2 hybrid, there are three extra peaks at about 1106, 1717, and 1733 cm^{-1} in its FTIR spectrum

[Figs. 3(D) and 4(D)]. The peak at 1106 cm^{-1} indicates the Ti—O—C bond, which may be produced from the reaction between PLA-*g*-AA and the titanium-bonded isopropyl group.[34,36] Furthermore, the PLA-*g*-AA/TiO_2 hybrid also produced a broad O—H bond stretching at about 3000–3300 cm^{-1} [Fig. 2(D)]. This was due to the formation of hetero-associated hydrogen bonds between carboxylic acid groups of PLA-*g*-AA and titanol groups of the titania network in the hybrid.[37] The expansion of the FTIR spectra in the limited range of 1700–1800 cm^{-1} (Fig. 3) more clearly illustrates the difference between the spectra with and without AA grafted onto the polymer. The PLA spectrum [Fig. 3(A)] shows only a strong, broad —C=O stretching vibration band at 1700–1760 cm^{-1} centered at 1753 cm^{-1}, whereas the PLA-*g*-AA spectrum [Fig. 3(B)] shows an extra peak at 1710 cm^{-1} caused by the grafting of AA onto PLA. However, PLA-*g*-AA in the PLA-*g*-AA/TiO_2 hybrid loses its peak at 1710 cm^{-1} and gains two new peaks at 1733 and 1717 cm^{-1} [Fig. 4(D)]. This result may be due to the formation of ester groups through the reaction between carboxylic acid groups of PLA-*g*-AA and titanol groups of the titania network.[14,38–41]

To understand the effect of starch on the biodegradable hybrids, FTIR spectroscopy was used to examine PLA/starch (20 wt %), PLA-*g*-AA/starch (20 wt %), and PLA-*g*-AA/TiO_2 (10 wt %)/starch (20 wt %), and the results are illustrated in Figure 5(A–C), respectively. In Figure 5, all the characteristic peaks of PLA can be seen in the three polymers. It is also found that broad O—H bond stretching at 3000–3300 cm^{-1} appears in the FTIR spectra of the three blends. This is because of the —OH group of starch for the bond stretching vibration. A similar result can be found in some articles.[27,42] For the case of PLA-*g*-AA/starch (20 wt %) [Fig. 5(B)], besides the common peaks appearing in the spectrum of the PLA/starch (20 wt %) blend, there is a new absorption peak (at ca. 1737 cm^{-1}) corresponding to the ester carbonyl stretching vibration in the copolymer. The appearance of this new absorption peak is perhaps due to the formation of an ester carbonyl functional group from the reaction between the —OH group of starch and the —COOH group of PLA-*g*-AA.[43,44] On the basis of this result, one can infer that branched and crosslinked macromolecules may be produced in PLA-*g*-AA/starch because the copolymer has carboxyl groups to react with the hydroxyl groups of the starch. From the results of Figure 5(B,C), it can be seen that some extra peaks (1600–1650, 1106, and 800–850 cm^{-1}) appear in the FTIR spectrum of the PLA-*g*-AA/TiO_2 (10 wt %)/starch (20 wt %) hybrid. As discussed previously, those extra peaks are due to the characteristic frequencies of TiO_2 and the formation of the Ti—O—C bond.

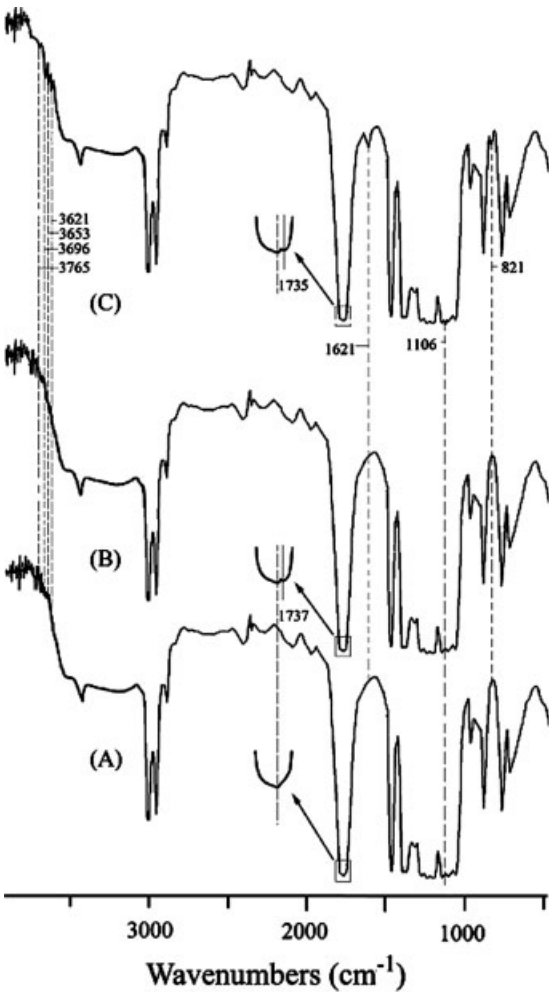

Figure 5 FTIR spectra of (A) PLA/starch (30 wt %), (B) PLA-*g*-AA/starch (30 wt %), and (C) PLA-*g*-AA/TiO_2 (9.6 wt %)/starch (30 wt %).

Hybrid morphology

To prove the formation of nanocomposites and to study the distribution and size of starch in the polymer matrix, the tensile fractured surfaces of hybrids were examined with SEM. The SEM microphotographs of PLA and PLA-*g*-AA/TiO_2 are presented in Figure 6. The white beads denote the titania particles, whereas the dark areas represent the polymer matrix. Excess titania particles aggregate into larger clusters, and the occurrence of phase separation is then realized for higher contents of TiO_2 (e.g., 10 wt %). The SEM microphotographs with a magnification of 300× for the fractured surfaces of PLA, PLA/starch, PLA-*g*-AA/starch, and PLA-*g*-AA/TiO_2/starch are shown in Figure 7. It was found that the phase size (ca. 1.2 ± 0.1 μm) of starch in PLA-*g*-AA/TiO_2/starch (30 wt %) was smaller than that (ca. 2.0 ± 0.2 μm) in PLA-*g*-AA/starch (30 wt %).With different starch contents, the average pore diameter, which is the phase size of starch, of fractured surfaces

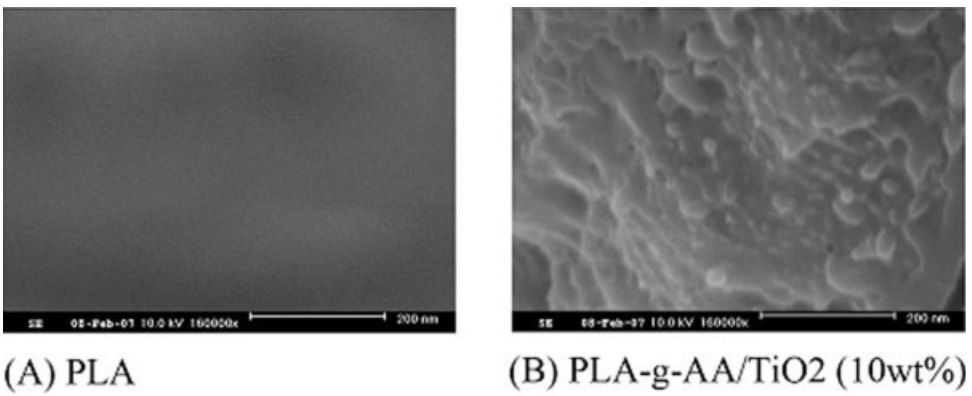

Figure 6 SEM micrographs of the pure PLA and PLA-*g*-AA/TiO_2 hybrid.

of hybrids (PLA-*g*-AA/starch and PLA-*g*-AA/TiO_2/starch) is summarized in Table II. The phase size of starch increased with an increasing content of starch, and the PLA-*g*-AA/TiO_2/starch hybrid had a smaller phase size than the other two. It was realized that the large phase size of starch produced the suggested poor adhesion and compatibility between the starch and polymer matrix. Therefore, the PLA-*g*-AA/TiO_2/starch hybrid provided the best dispersion and homogeneity of starch in the polymer matrix.

Thermal stability of the hybrids (DSC and TGA tests)

The thermal properties of hybrids with various TiO_2 contents were obtained via DSC and TGA tests. T_m and T_g of PLA and PLA/TiO_2 hybrids were determined from the DSC heating thermograms (Fig. 8), and the results are summarized in Figure 9. T_g of the hybrids is associated with a cooperative motion of long-chain segments, which may be hindered by TiO_2. Therefore, as expected, PLA-*g*-AA/TiO_2

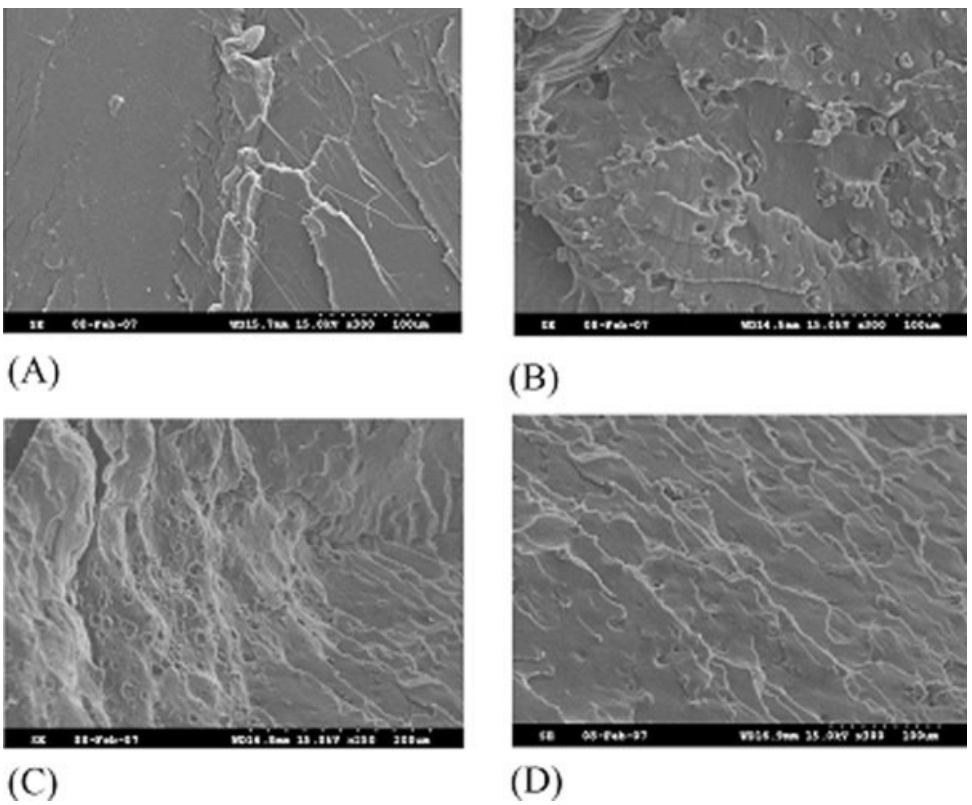

Figure 7 SEM micrographs of (A) pure PLA, (B) PLA/starch (30 wt %), (C) PLA-*g*-AA/starch (30 wt %), and (D) PLA-*g*-AA/TiO_2 (9.6 wt %)/starch (30 wt %).

TABLE II
TGA Data of the PLA-*g*-AA/TiO_2 Nanocomposites

TiO_2 (wt %)	$T_{d,\text{initial}}$ (°C)	$T_{d,\max}$ (°C)	$Wt_{R,600}$ (%)
0	268	338	0.77
3	291	353	4.22
7	323	371	6.85
10	348	389	10.31
12	358	385	12.31
15	375	380	14.95

recorded higher T_g values than the PLA-*g*-AA copolymer (Fig. 9). It may be suggested that the increase in T_g for PLA-*g*-AA/TiO_2 hybrids is due to the fact that the TiO_2 phase was able to form chemical bonds on hydroxyl group sites provided by the carboxylic acid groups of PLA-*g*-AA. These strong bonds are able to hinder the motion of the polymer chains. The enhancement of T_g was not marked for the TiO_2 content beyond 10 wt %. This result might be due to the low grafting percentage (ca. 5.96 wt %) of the PLA-*g*-AA copolymer because the increment of T_g is dependent on the number of functional groups in the copolymer matrix able to react with the hydroxyl groups in TiO_2.[45] With the TiO_2 content above 10 wt %, they were dispersed physically in the polymer matrix. Such excess TiO_2 might have caused separation of the organic and inorganic phases and lowered their compatibility, causing the slight enhancement of the T_g value. Figure 9 also shows that T_m decreased markedly with increasing TiO_2 content up to 10 wt %, and then the effect was slight. The marked decrease in T_m of PLA-*g*-AA/TiO_2 was probably the result of TiO_2 prohibiting the movement of the polymer segments, causing polymer chain arrangement to become more difficult, and also of the hydrophilic character of TiO_2, which led to poor adhesion with the hydrophobic PLA.

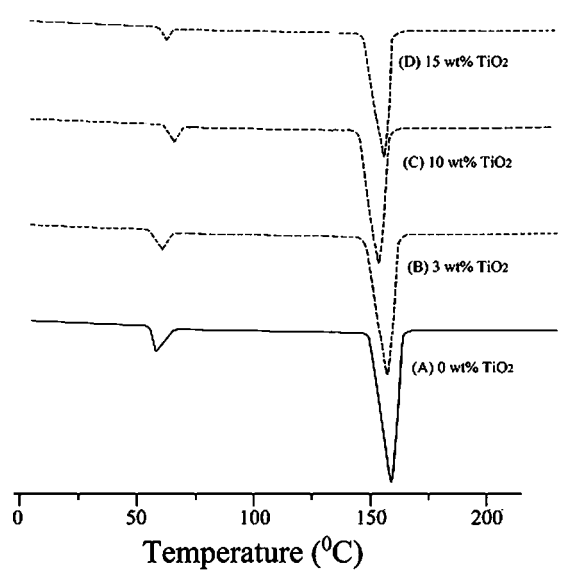

Figure 8 DSC heating thermograms of the PLA-*g*-AA/TiO_2 hybrids with different TiO_2 contents.

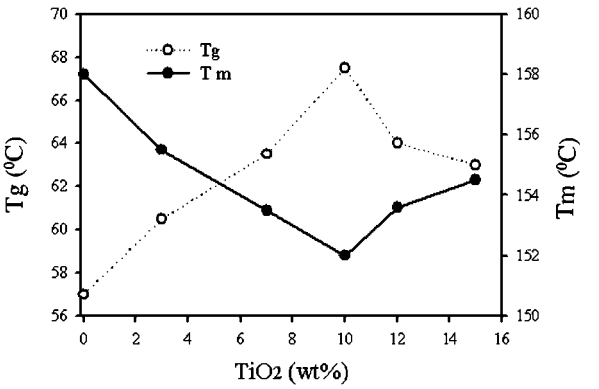

Figure 9 T_m and T_g versus the TiO_2 content for the PLA-*g*-AA/TiO_2 blends.

In this study, we used TGA to determine the effect of the TiO_2 content on the thermal stability of hybrids via the measurement of the weight percentage of the residue at 600°C ($Wt_{R,600}$), $T_{d,\text{initial}}$, and $T_{d,\max}$ from thermogravimetry percentage and derivative thermogravimetry curves (not shown here), and the results are illustrated in Table II. The $T_{d,\text{initial}}$ values of PLA-*g*-AA and hybrids with TiO_2 contents of 0, 3, 7, 10, 12, and 15 wt % were 268, 291, 323, 348, 358, and 375°C, respectively. Similar to the results of some articles,[46–48] $T_{d,\max}$ also increased with the TiO_2 content increasing up to 10 wt % and then decreased slightly because of the agglomeration tendency of TiO_2. As a result, the nanocomposites possessed higher thermal stability than the PLA-*g*-AA copolymer. The increase in $T_{d,\text{initial}}$ and $T_{d,\max}$ was probably caused by the increased difficulty in arranging the polymer chains due to TiO_2 prohibiting the movement of the polymer segments. Another potential cause was the character of TiO_2, which would lead to a condensation reaction with PLA-*g*-AA. Bian et al.[49] studied the properties of clay nanocomposites and blends with polyaniline/TiO_2 and reported similar phenomena. The enhancement of the thermal stability can also be attributed to the shielding effect of TiO_2 nanoparticles against the volatile products generated during thermal decomposition. According to these TGA traces, the increment of $T_{d,\text{initial}}$ was about 80°C for 10 wt % TiO_2 but was only 35°C as the TiO_2 content was increased from 10 to 15 wt %. This result further confirmed that the optimal loading of TiO_2 was 10 wt % because excess TiO_2 would cause separation of the organic and inorganic phases and lower their compatibility. $Wt_{R,600}$ increased from 0.77 to 14.95 wt % with TiO_2 loadings of 0–15 wt %. The enhancement of the char formation was ascribed to the high heat resistance exerted by titania itself.[47]

Mechanical properties of the hybrids

The stress–strain curves of the PLA-*g*-AA/TiO_2 nanocomposites with different TiO_2 contents are shown in Figure 10. In all cases, the curves are linear at a low strain, and this is followed by plastic deformation in the region of 2% strain. At higher strains, the films yielded up to a breaking strain of 4% for PLA-*g*-AA. This breaking strain tended to decrease with increasing TiO_2 content and occurred at about 2.0% for the 15 wt % composite; this was followed by a stiffening of the material. This behavior may be due to strain-induced crystallization of the polymer resulting in material hardening.[50] Similarly to the effect of the TiO_2 content on the thermal property, it can be seen from Figure 10 that the tensile strength of PLA-*g*-AA/TiO_2 hybrids increased rapidly with the TiO_2 content increasing from 0 to 10 wt %, and then the tensile strength improved slightly. The positive effect on the tensile strength may be due to the stiffness of the TiO_2 layers contributing to the presence of immobilized or partially immobilized polymer phases,[51] the high aspect ratio and surface area of TiO_2, and the nanoscale dispersion of TiO_2 particles in the polymer matrix. It is also possible that TiO_2 orientation and molecular orientation contributed to the observed reinforcement effect. The slight decrement in the tensile strength for TiO_2 contents above 10 wt % could be attributed to the inevitable aggregation of the TiO_2 particles at higher TiO_2 contents. These results support the theoretical and molecular simulation predictions that the stress transfer and hence strength of inorganic polymer composites can be effectively increased by the formation of chemical bonding between them.[52,53]

Figure 11 shows the variations of the tensile strength at break with the starch content for PLA/starch, PLA-*g*-AA/starch, and PLA-*g*-AA/TiO_2/starch blends. The tensile strength and elongation of pure PLA both decreased when it was grafted with

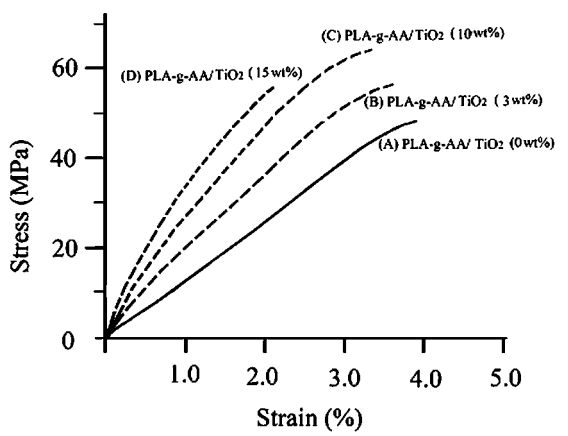

Figure 10 Representative stress–strain curves for the PLA-*g*-AA/TiO_2 hybrids with different TiO_2 contents.

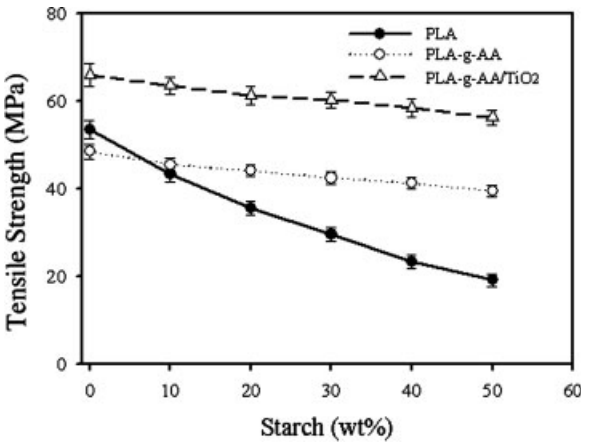

Figure 11 Tensile strength at break versus the starch content for the PLA, PLA-*g*-AA, and PLA-*g*-AA/TiO_2 blends.

AA. To further understand the dispersibility of starch in these three blends with different starch contents, the starch phase size was obtained from the SEM micrographs of the respective blends, and the results are summarized in Table III. For PLA/starch blends, the tensile strength at break decreased continuously and markedly from 53.5 to 19.2 MPa as the starch content was increased from 0 to 50 wt % (the black and solid circular symbols in Fig. 11). Table II also shows that the starch phase size of PLA/starch blends increased remarkably with increasing starch content. As might be expected, the PLA/starch blends showed poor mechanical properties because of low adhesion and dispersiveness between the two immiscible phases (hydrophobic PLA and hydrophilic starch). It is evident that the mechanical properties strongly depended on the dispersion and phase size of starch in the PLA matrix because the larger starch phase size gave poorer adhesion and compatibility between starch and PLA. Therefore, the deterioration in the mechanical properties of PLA/starch blends could be explained by the fact that the starch phase size of the PLA/starch blends increased with increasing starch content.

For PLA-*g*-AA/starch blends, as shown by the open circular symbols in Figure 11, a quite different

TABLE III
Starch Phase Size of the PLA/Starch, PLA-*g*-AA/Starch, and PLA-*g*-AA/TiO_2/Starch Blends with Different Starch Contents

	Phase size (μm)		
Starch (wt %)	PLA/ starch	PLA-*g*-AA/ starch	PLA-*g*-AA/ TiO_2/starch
10	2.3 ± 0.2	1.3 ± 0.1	0.8 ± 0.1
20	3.0 ± 0.3	1.6 ± 0.2	1.0 ± 0.1
30	3.8 ± 0.4	2.0 ± 0.2	1.2 ± 0.1
40	4.5 ± 0.5	2.3 ± 0.3	1.5 ± 0.2
50	5.1 ± 0.6	2.6 ± 0.3	1.8 ± 0.3

behavior of the tensile strength at break could be found; that is, the tensile strength at break of the PLA-*g*-AA/starch blends decreased slightly with increasing starch content, although PLA-*g*-AA had a lower value of the tensile strength than the pure PLA. It was also found that the PLA-*g*-AA/starch blends not only showed larger values of the tensile strength than those of the PLA/starch blends but also provided stable values of the tensile strength when the starch content was beyond 10 wt %. A contribution to this result may be the better dispersion and smaller phase size of starch in the PLA-*g*-AA matrix (Table II). This better dispersion may arise from the formation of branched and crosslinked macromolecules because this PLA-*g*-AA copolymer has carboxylic acid groups to react with the hydroxyls of starch. These macromolecules have higher tensile strength in comparison with the linear ones.

For PLA-*g*-AA/TiO_2/starch blends (the open triangular symbols in Fig. 11), in comparison with PLA/starch and PLA-*g*-AA/starch blends, much enhancement of the values of the tensile strength at break can be observed. The much better mechanical properties provided by the PLA-*g*-AA/TiO_2/starch blends may have come from the much smaller starch phase size, the nanoscale dispersion of silicate layers in the polymer matrix, and the formation of the Ti—O—C bond from the reaction between PLA-*g*-AA and the silicate phase of TiO_2.

CONCLUSIONS

Organic–inorganic hybrid materials were prepared via *in situ* polymerization of TTIP in the presence of starch and PLA (or PLA-*g*-AA). The FTIR spectra verified that AA had been grafted onto the PLA copolymer and that Ti—O—C bonds were formed in the PLA-*g*-AA/TiO_2 hybrid. The newly formed chemical bonds may have been produced through the dehydration of carboxylic acid groups in the PLA-*g*-AA matrix with titanol groups in the titania network. For PLA-*g*-AA/starch and PLA-*g*-AA/TiO_2/starch hybrids, it was also found that an ester carbonyl functional group may have been formed from the reaction between the —COOH group of PLA-*g*-AA and the —OH group of starch. TGA tests showed that the PLA-*g*-AA/TiO_2 hybrids produced higher values of $T_{d,\text{initial}}$ and $T_{d,\max}$ than the equivalent PLA/TiO_2 ones. Meanwhile, the maximum tensile strength and T_g values occurred at about 10 wt % TiO_2 for PLA-*g*-AA/TiO_2 hybrids. Above 10 wt % TiO_2, it is proposed that excess titania particles may cause separation between the organic and inorganic phases, thus reducing compatibility between the titania network and PLA-*g*-AA. However, with the PLA-*g*-AA chains chemically end-linked into the inorganic network, the shifts in T_g were much larger because of the interfacial forces of PLA-*g*-AA/TiO_2 associated with the Ti—O—C and hetero-associated hydrogen bonds. To improve the biodegradable property of the PLA/TiO_2 hybrids, starch was chosen as the organic filler, and the result showed that PLA-*g*-AA/TiO_2/starch hybrids could markedly improve the thermal and mechanical properties of PLA/starch and PLA-*g*-AA/starch hybrids because the nanoscale dispersion of titania particles, the smallest starch phase size, and the primary valence forces could be obtained in the PLA-*g*-AA/TiO_2/starch hybrids. Finally, the biodegradable PLA-*g*-AA/clay/starch nanocomposites produced in our laboratory could provide a plateau tensile strength at break when the starch content was up to 50 wt %.

References

1. Lu, X.; Zhao, Q.; Liu, X.; Wang, D.; Zhang, W.; Wang, C.; Wei, Y. Macromol Rapid Commun 2006, 27, 430.
2. Wu, C. S. J Polym Sci Part A: Polym Chem 2005, 43, 1690.
3. Xing, Y.; Ding, X. J Appl Polym Sci 2007, 103, 3113.
4. Kim, H.-W.; Kim, H.-E.; Salih, V.; Knowles, J. C. J Biomed Mater Res B 2005, 72, 1.
5. Gianni, A. D.; Trabelsi, S.; Rizza, G.; Sangermano, M.; Althues, H.; Kaskel, S.; Voit, B. Macromol Chem Phys 2007, 208, 76.
6. Deffar, D.; Teng, G.; Soucek, M. D. Macromol Mater Eng 2001, 286, 204.
7. Fattakhova-Rohlfing, D.; Wark, M.; Brezesinski, T.; Smarsly, B. M.; Rathouský, J. Adv Funct Mater 2007, 17, 123.
8. Choi, H.; Sofranko, A. C.; Dionysiou, D. D. Adv Funct Mater 2006, 16, 1067.
9. Koelsch, M.; Cassaignon, S.; Guillemoles, J. F.; Joliver, J. P. Thin Solid Films 2002, 430–404, 312.
10. Wu, C. S.; Liao, H. T. J Polym Sci Part B: Polym Phys 2003, 41, 351.
11. Que, W.; Zhou, Y.; Lam, Y. L.; Chan, Y. C.; Kam, C. H. Thin Solid Films 2000, 358, 16.
12. Hench, L. L.; West, J. K. Chem Rev 1990, 90, 33.
13. Slooff, L. H.; Kroon, J. M.; Loos, J.; Koetse, M. M.; Sweelssen, J. Adv Funct Mater 2005, 15, 689.
14. Liao, H. T.; Wu, C. S. J Polym Sci Part B: Polym Phys 2004, 42, 4272.
15. Mark, J. E. Polym Eng Sci 1996, 36, 2905.
16. Perrin, F. X.; Nguyen, V. N.; Vernet, J. V. Macromol Chem Phys 2005, 206, 1439.
17. Siuzdak, D. A.; Start, P. R.; Mauritz, K. A. J Appl Polym Sci 2000, 77, 2832.
18. Martin, O.; Averous, L. Polymer 2001, 42, 6209.
19. Elvassore, N.; Bertucco, A.; Caliceti, P. J Pharm Sci 2001, 90, 1628.
20. Piorkowska, E.; Kulinski, Z. Polymer 2005, 46, 10290.
21. Cho, S. M.; Kim, S. Y.; Lee, Y. M.; Sung, Y. K.; Cho, C. S. J Appl Polym Sci 1999, 73, 2151.
22. Tsuji, H.; Ikada, Y. J Appl Polym Sci 1998, 67, 405.
23. You, Y.; Lee, S. W.; Youk, J. H.; Min, B. M.; Lee, S. J.; Park, W. H. Polym Degrad Stab 2005, 90, 441.
24. Shi, Z.; Zhou, Y.; Yan, D. Polymer 2006, 47, 8073.
25. Ferreira, B. M. P.; Zavaglia, C. A. C.; Duek, E. A. R. J Appl Polym Sci 2002, 86, 2898.
26. Gaylord, N. G.; Metha, R.; Kumar, V.; Taze, M. J Appl Polym Sci 1989, 38, 359.
27. Wu, C. S. Macromol Bio 2005, 5, 352.

28. Wu, C. S.; Liao, H. T. Polymer 2005, 46, 10017.
29. Tsuji, H.; Fukui, I.; Daimon, H.; Fujie, K. Polym Degrad Stab 2003, 81, 501.
30. Kumar, P. M.; Badrinarayanan, S.; Sastry, M. Thin Solid Films 2000, 358, 122.
31. Shogren, R. L.; Thompson, A. R.; Felker, F. C.; Harry-Okuru, R. E.; Gordon, S. H.; Greeen, R. V.; Gould, J. M. J Appl Polym Sci 1992, 44, 1971.
32. Yao, F.; Chen, W.; Wang, H.; Lin, H.; Yao, K.; Sun, P.; Lin, H. Polymer 2003, 44, 6435.
33. Kim, J.; Tirrell, D. A. Macromolecules 1999, 32, 945.
34. Chiang, P. C.; Whang, W. T. Polymer 2003, 44, 2249.
35. Shao, P. L.; Mauritz, K. A.; Moore, R. B. J Polym Sci Part B: Polym Phys 1996, 34, 873.
36. Zhang, J.; Wang, B. J.; Ju, X.; Lin, T.; Hu, T. D. Polymer 2001, 42, 3697.
37. Hsu, Y. G.; Lin, F. J. J Appl Polym Sci 2000, 75, 275.
38. Steunou, N.; Robert, F.; Boubekeur, K.; Ribot, F.; Sanchez, C. Inorg Chim Acta 1998, 279, 141.
39. Langel, W.; Menken, L. Surf Sci 2003, 538, 1.
40. Robert, D.; Weber, J. V. Adsorption 2000, 6, 175.
41. Bikiaris, D.; Karavelidis, V.; Karayannidis, G. Macromol Rapid Commun 2006, 27, 1199.
42. Wu, C. S.; Laio, H. T. J Appl Polym Sci 2002, 86, 1792.
43. Wu, C. S. Polym Degrad Stab 2003, 80, 127.
44. Bikiaris, D.; Panayiotou, C. J Appl Polym Sci 1998, 70, 1503.
45. Huang, Z. H.; Qju, K. Y. Polymer 1997, 38, 521.
46. Pluta, M.; Galeski, A.; Alexandre, M.; Paul, M.-A.; Dubois, P. J Appl Polym Sci 2002, 86, 1497.
47. Ou, C.-F. J Polym Sci Part B: Polym Phys 2003, 41, 2902.
48. Zhang, J. H.; Zhuang, W.; Zhang, Q.; Liu, B.; Hu, B. X.; Shen, J. Polym Compos 2007, 28, 545.
49. Bian, C.; Yu, Y.; Xue, G. J Appl Polym Sci 2007, 104, 21.
50. Coleman, J. N.; Cadek, M.; Blake, R.; Nicolosi, V.; Ryan, K. P.; Belton, C.; Fonseca, A.; Nagy, J. B.; Cun'ko, Y. K.; Blau, W. J. Adv Funct Mater 2004, 14, 791.
51. Zhang, X.; Liu, T.; Sreekumar, T. V.; Kumar, S.; Moore, V. C.; Hauge, R. H.; Smalley, R. E. Nano Lett 2003, 3, 1285.
52. Geng, H.; Rosen, R.; Zheng, B.; Shimoda, H.; Fleming, L.; Liu, J.; Zhou, O. Adv Mater 2002, 14, 1387.
53. Yao, Z.; Braidy, N.; Botton, G. A.; Adronov, A. J Am Chem Soc 2003, 125, 16015.